

Article

Multifunctional 3D-Printed Thermoplastic Polyurethane (TPU)/Multiwalled Carbon Nanotube (MWCNT) Nanocomposites for Thermal Management Applications

Daniele Rigotti , Andrea Dorigato and Alessandro Pegoretti 

Department of Industrial Engineering and INSTM Research Unit, University of Trento, Via Sommarive 9, 38123 Trento, Italy; andrea.dorigato@unitn.it (A.D.); alessandro.pegoretti@unitn.it (A.P.)

* Correspondence: daniele.rigotti-1@unitn.it

Featured Application: This work on 3D-printed TPU/MWCNT/PCM composites offers information on materials with significant potential for applications in advanced thermal management systems. These materials can be employed in smart textiles, wearable electronics, or flexible sensors, where precise control over temperature regulation and thermal conductivity is essential. These composites' enhanced electrical conductivity and tunable thermal properties make them promising candidates for multifunctional devices that require efficient heat dissipation, strain sensing, or even self-regulating thermal insulation.

Abstract: In this work, multiwalled carbon nanotubes (MWCNTs) were melt-compounded into a novel thermal energy storage system consisting of a microencapsulated paraffin, with a melting temperature of 6 °C (M6D), dispersed within a flexible thermoplastic polyurethane (TPU) matrix. The resulting materials were then processed via Fused Filament Fabrication (FFF), and their thermo-mechanical properties were comprehensively evaluated. After an optimization of the processing parameters, good adhesion between the polymeric layers was obtained. Field-Emission Scanning Electron Microscopy (FESEM) images of the 3D-printed samples highlighted a uniform distribution of the microcapsules within the polymer matrix, without an evident MWCNT agglomeration. The thermal energy storage/release capability provided by the paraffin microcapsules, evaluated through Differential Scanning Calorimetry (DSC), was slightly lowered by the FFF process but remained at an acceptable level (i.e., >80% with respect to the neat M6D capsules). The novelty of this work lies in the successful integration of MWCNTs and PCMs into a TPU matrix, followed by 3D printing via FFF technology. This approach combines the high thermal conductivity of MWCNTs with the thermal energy storage capabilities of PCMs, creating a multifunctional nanocomposite material with unique thermal management properties.

Keywords: thermoplastic polyurethane; phase-change materials; carbon nanotubes; 3D printing; fused filament fabrication; thermal energy storage



Citation: Rigotti, D.; Dorigato, A.; Pegoretti, A. Multifunctional 3D-Printed Thermoplastic Polyurethane (TPU)/Multiwalled Carbon Nanotube (MWCNT) Nanocomposites for Thermal Management Applications. *Appl. Sci.* **2024**, *14*, 9614. <https://doi.org/10.3390/app14209614>

Academic Editor: Andrea Frazzica

Received: 26 September 2024

Revised: 14 October 2024

Accepted: 18 October 2024

Published: 21 October 2024



Copyright: © 2024 by the authors. Licensee MDPI, Basel, Switzerland. This article is an open access article distributed under the terms and conditions of the Creative Commons Attribution (CC BY) license (<https://creativecommons.org/licenses/by/4.0/>).

1. Introduction

Thermoplastic polyurethane (TPU) is a polymer with an elasticity close to that of rubber but with better durability and toughness, and it is thus widely used in coatings, adhesives, thermoplastic elastomers, and sport equipment [1,2]. Unfortunately, like most polymers, TPU presents low thermal conductivity, constraining its effectiveness for thermal management applications [3]. This problem is commonly faced in the development of plastic heat exchangers, for which the cheapness, low density, and elevated corrosion resistance of TPU are negatively counterbalanced by its intrinsically poor thermal conductivity [4]. On the other hand, nanostructured carbon fillers have attracted much interest due to their high thermal conductivity, which, for carbon nanotubes, is higher than 3000 W/K m at

room temperature [5]. Carbon nanotubes are known as one of the stiffest manmade materials; moreover, their outstanding electrical and thermal conductivity have generated a lot of interest in the production of MWCNT-based nanocomposites with enhanced multifunctionality [6]. According to the literature, electrical and mechanical properties can be substantially improved by the incorporation of MWCNTs into the TPU matrix [7–9]. For instance, researchers have been actively exploring electrically conductive polymer nanocomposites for advanced strain-sensing applications. Bharadwaj et al. reported the development of flexible and conductive nanocomposite strain sensors based on TPU [10]. By incorporating MWCNTs using a solution-mixing process and high-speed homogenization, they achieved an electrical percolation threshold as low as 0.1 wt%, thus obtaining a sensing material with an instantaneous gauge factor of 1389 at 50% strain. Furthermore, cyclic stress/release experiments underscored the robust recoverability and reproducibility of the strain-sensing effect. Yun et al. tackled the challenge of maintaining the electrical conductivity of TPU nanocomposites during stretching, a crucial requirement for next-generation flexible electronics [11]. They developed highly stretchable and conductive MWCNT/TPU composite foams using a novel approach that involved melt-compounding, supercritical fluid treatment, and physical foaming. The introduction of a microcellular structure effectively suppressed the increase in electrical resistance during stretching. This approach not only preserved electrical conductivity but also enhanced the material elongation capability, opening the way for the development of stretchable and conductive polymeric materials for advanced electronics. Wang et al. focused their attention on the fabrication of MWCNT/TPU electrospun films for strain sensing [12]. By varying the MWCNT content (from 10 up to 15 wt%) in electrospun nanofiber films, they observed improved electrical conductivity and enhanced strain-sensing capabilities. The MWCNT/TPU nanofiber film with a MWCNT content of 10% showed a gauge factor (GF) of 10.14 at 20% strain. With 12.5% MWCNTs, the strain-monitoring range was extended from 1% to 40%, with a GF of about 2.06. The sensor with this composition could measure pressures ranging from 0 to 220 kPa, with a linear sensitivity of approximately 0.432 kPa^{-1} in the 0–5 kPa range. Moreover, nanocomposite films with a MWCNT loading of 12.5 wt% exhibited rapid responsiveness and excellent dimensional stability. These findings suggest the potential of these materials for use in human motion and pressure detection, highlighting the prospects of intelligent wearability. Kumar et al. presented a study detailing the development of robust, stretchable, and highly sensitive TPU nanocomposites filled with MWCNTs to be applied as piezoresistive strain-sensing materials [13]. The uniform dispersion of MWCNTs within the TPU matrix led to a notably low percolation threshold (0.1 wt%) and exceptional electrical conductivity. The strain-sensing capability of these materials was strongly correlated with the MWCNT concentration. Moreover, this study reported enhancements in the tensile strength, yield strength, and Young's modulus equal to 10%, 83%, and 66%, respectively, for a MWCNT loading of 0.3 wt%. Cyclic stretch/release tests on these nanocomposites conducted by applying a strain amplitude of 50% showed good strain-sensing recoverability and reproducibility at up to 100 cycles.

Fused Filament Fabrication (FFF) is one of the most popular additive manufacturing technologies [14]. The 3D-printed object is built up layer by layer, controlling the deposition of the molten feed stock material. Several investigations have recently been undertaken to explore the realm of additive manufacturing, with an additional focus on the fabrication of polymer/MWCNT nanocomposite structures through the FFF technique [15]. Many of these studies have delved into the intricate details of this additive manufacturing technology, seeking to unravel its potential for producing multifunctional complex-shape structures by seamlessly merging polymer matrices with the exceptional electrical and mechanical properties provided by MWCNTs [16–21]. Therefore, in the last few years, researchers have explored the integration of sensing capabilities into soft robotics using 3D-printed flexible TPU/MWCNT composites. Hohimer et al. employed multi-material FFF to print these composites and investigated their microstructures, electrical conductivity, capacitive-sensing, and piezoresistive-sensing properties [22]. The effect of layer height

on conductivity varied with the MWCNT content. For the TPU-2 wt.% MWCNT samples, layer height had no significant effect on conductivity, likely due to the proximity to the percolation threshold. In contrast, the TPU-3 wt.% MWCNT samples showed a strong correlation between layer height and conductivity, with decreasing layer height increasing conductivity by reducing interfacial resistance. Both through-line and in-line samples with 4 wt.% MWCNTs exhibited an overall increase in conductivity with an increasing layer height, a property attributed to the larger cross-sectional area creating more percolation pathways. The effect of raster pattern and sample size on conductivity was evident in the TPU-3 wt.% MWCNTs samples at different layer heights. [23]. While bed temperature could affect internal void fraction and bond neck growth between rasters, the low glass transition temperature of TPU ($-38\text{ }^{\circ}\text{C}$) made the practical range of bed temperatures ($35\text{--}95\text{ }^{\circ}\text{C}$) insignificant with respect to raster-to-raster bonding and conductivity. Similarly, Christ et al. developed 3D-printable, flexible, and conductive thermoplastic materials for strain-sensing applications [24]. They combined TPU with MWCNTs, and the extruded filaments were processed through FFF to produce 3D-printed sensors. Their investigation revealed enhanced stiffness due to the inclusion of MWCNTs and excellent interlayer adhesion, accompanied by a modest decrease in elastic modulus ($\sim 14\%$). The electrical conductivity trends in both the through-layer and cross-layer directions of the 3D-printed samples closely resembled those of hot-pressed samples. Interestingly, increasing the MWCNT content in the printed samples led to slightly higher cross-layer conductivity, likely due to orientation effects imparted during printing. This effect was more significant near the percolation threshold. Exceptional piezoresistive gauge factors of up to 176 were achieved under a strain level of 100%, with high repeatability under cyclic loading conditions. Therefore, TPU/MWCNT systems were determined to be a promising 3D-printing material for applications in wearable electronics, soft robotics, and prosthetics, allowing complex shape design and elevated customization potential. Kim et al. introduced an innovative method for the direct fabrication of 3D multiaxial force sensors using FFF applied to functionalized nanocomposite filaments [25]. Their approach involved creating a 3D cubic cross-shaped force sensor capable of measuring forces along three axes. This sensor had two components: a structural part made of a TPU filament and a sensing part made of a TPU/MWCNT nanocomposite filament with surface piezo-resistivity. These parts were produced simultaneously using 3D printing. This method allowed customization and quick production and was cost-effective, allowing for the direct fabrication of multiaxial sensors without additional assembly or integration.

PCMs are widely employed for various applications, especially for enhancing the thermal comfort of buildings, in solar heating systems, in thermal protection systems, air-conditioning, transportation, electronic devices, thermal regulated textiles, etc. Nowadays, PCMs are integrated into fabrics and clothes to regulate skin temperature, thereby increasing thermal comfort and/or alleviating heat strain [26–29]. These materials can absorb excess body heat generated during physical activity and release it when needed, thus maintaining a stable temperature for the wearer. For instance, PCM-treated active wear is designed to balance the heat produced by the body with the heat released into the environment, which is crucial to prevent thermal stress during intense sports activities [27,28]. Specific applications include gloves for ice climbing and cycling, wherein PCM's ability to regulate temperature can improve comfort and performance. The incorporation of PCMs into sports textiles not only enhances thermal regulation but also contributes to the overall functionality and comfort of the garments used in various athletic activities [30]. Additionally, mathematical modeling indicated that wearing a PCM cooling vest could substantially decrease body heat load, highlighting the vest's role in enhancing thermal comfort [31]. Furthermore, the effectiveness of PCMs in reducing thermal strain has been corroborated by various studies, which noted that the cooling effect is influenced by factors such as vest design and environmental conditions [32,33].

In the last few years, our research group focused its attention on the development of multifunctional 3D-printable TPU-based materials with thermal energy storage (TES)

capability thanks to the addition of microcapsules filled with paraffin [34,35]. The encapsulation of Phase-Change Materials (PCMs), able to absorb/release thermal energy as latent heat upon a phase change, has opened a new route for fabricating smart materials with improved multifunctionality [36].

In the previous work performed by our group, we highlighted the possibility of successfully printing TPU blends with 40 wt% PCM through FFF technology, yielding multifunctional materials with good thermal energy storage efficiency and suitable mechanical properties [37]. In this sense, the addition of a conductive nanofiller within the TPU matrix could enhance the thermal and electrical conductivity of the resulting materials, giving rise to novel 3D-printed multifunctional structures that could be applied in smart electronics and sensors or in sport applications. This study introduces, for the first time, the development of 3D-printed TPU/MWCNT nanocomposite materials incorporating PCM for thermal management applications. Utilizing the FFF process, the integration of PCM and CNTs into TPU enhances the material's thermal properties. The 3D-printed samples, with varying quantities of PCM and MWCNTs, were thoroughly characterized to evaluate their morphological, thermal, and mechanical properties, marking a significant advancement in the field of thermal management.

2. Materials and Methods

2.1. Materials

Desmopan® 6064A TPU (density = 1.09 g/cm³, melting temperature = 200 °C) was kindly provided by Covestro Srl (Milano, Italy) in the form of pellets. This injection-molding-grade TPU is used in various applications, such as shoe soles and automotive interiors, due to its excellent mechanical properties, low abrasion tendency, complete lack of plasticizers, and microbial resistance. MWCNTs were provided by Nanocyl SA (Sambreville, Belgium) under the trade name Nanocyl NC7000TM. They were produced via catalytic chemical vapor deposition (CCVD) and supplied as a dry powder. The manufacturer's datasheet reported an average diameter of 9.5 nm and a length of 1.5 µm, a BET specific surface area of 250–300 m²/g, and a volume resistivity of 10^{−4} Ω·cm. Microtek MPCM6D microencapsulated paraffin (named M6D in this work), provided by Microtek Laboratories Inc. (Dayton, OH, USA), was utilized as PCM. In this PCM, paraffin wax characterized by a melting temperature (T_m) of 6 °C and a crystallization temperature (T_c) of about −10 °C was encapsulated inside a stable melamine formaldehyde polymeric shell. The resulting particles had a mean diameter of 17–20 µm and a density of 0.9 g/cm³ and were 85–90 wt% paraffin. Their melting enthalpy, according to the producer's datasheet, was in the interval of 157–167 J/g. All these materials were used as received.

2.2. Filament Extrusion

TPU granules and MWCNTs were melt-compounded in a Thermo Haake Rheomix 600 internal mixer, equipped with counter-rotating rotors operated at 200 °C and 60 rpm for 10 min, to obtain a material with 3 wt% carbon nanotubes that served as a masterbatch. Neat TPU granules and the desired amount of TPU/MWCNT masterbatch were finely ground and mixed with the paraffin microcapsules at room temperature using a mechanical stirrer for 5 min at 20 rpm to limit the leakage of paraffin from the capsules. The obtained mixtures were then extruded by using an Estru13 single-screw extruder provided by Friul Filiere SpA (Udine, Italy). This extruder was characterized by a screw diameter (D) of 14 mm, a screw length of 25D, and an extrusion die diameter of 3 mm. The screw rotation speed was set to 30 rpm, and the temperature profile varied from 105 °C in the feeding section up to 180 °C in the die zone. The temperature profile in the extruder was set such that the surface quality would be optimized and porosity inside the filaments would be avoided. Filaments with a constant diameter of about 1.75 mm, suitable for the 3D process, were thus obtained.

2.3. Preparation of 3D-Printed Samples

Next, 3D-printed specimens were prepared, using the extruded filaments as a starting material, by using a Sharebot Next-Generation desktop 3D printer (Sharebot, Nibionno, Italy) equipped with a 0.4 mm nozzle. An ISO 527 1BA dog bone specimen [38], with a gauge length of 25 mm, a width of 5 mm, and a thickness of 2 mm, suitable for tensile tests, was designed by using Autodesk Inventor Pro[®] 2023 software. The 3D model was then exported in .stl format, processed via Slicer[®], and exported in a GCODE format. A rectangular infill with a density of 100% was selected, while the infill angle was set to a 0°/0° configuration to maximize the density and the mechanical properties of the resulting samples. Considering that increasing the M6D and MWCNT content inside the TPU matrix made the printing stage more difficult, a feeding configuration with a 0° angle was the best choice for the preparation of the specimens. To avoid buckling in the feedstock material, the filament was cooled down with compressed air just before entering the nozzle [39], as shown in Figure 1. After several preliminary trials, the following parameters were set for the 3D-printing process: layer height = 0.20 mm, nozzle temperature = 240 °C, bed temperature = 40 °C, and deposition rate = 40 mm/s.

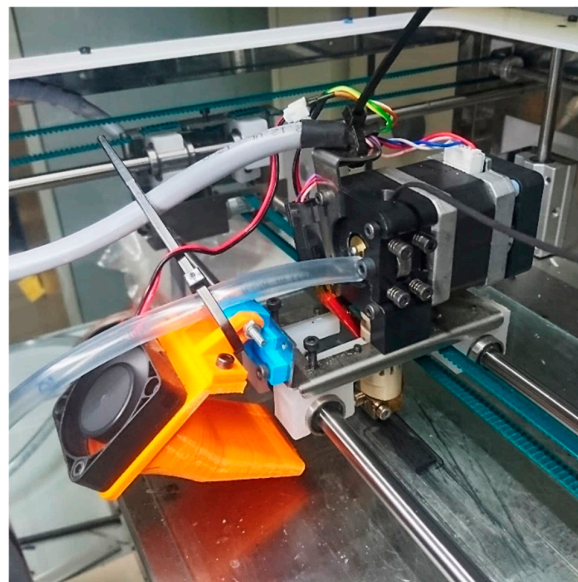


Figure 1. FFF machine equipped with a lab-made air-cooling system for the filament to avoid its failure via buckling.

2.4. Experimental Techniques

Microstructural observations of the cryo-fractured surfaces of the 3D-printed specimens were made to investigate the quality of the printing process and the interfacial interaction between microcapsules and the TPU matrix. A Zeiss Supra 40 (Zeiss, Oberkochen, Germany) high-resolution field-emission scanning electron microscope (FESEM), operated at an accelerating voltage of 2.5 kV was used. Samples were observed after the deposition of a thin platinum/palladium conductive coating on their surfaces.

Differential scanning calorimetry (DSC) measurements of the 3D-printed specimens were made by using a Mettler Toledo DSC30 calorimeter (Mettler, OH, USA). Specimens with a mass of about 10 mg were analyzed under a nitrogen flow of 150 mL/min, applying a first heating run from −100 to 220 °C, followed by a cooling step from 220 °C to −100 °C and a second heating run until 220 °C. All these scans were performed at 10 °C/min. The glass transition temperature (T_g) of TPU was evaluated as the inflection point in DSC thermogram, while the melting (T_m) and the crystallization (T_c) temperatures of M6D capsules within the nanocomposites were determined in accordance with the endothermic and exothermic peaks, respectively. The specific melting enthalpy (ΔH_m) and crystal-

lization enthalpy (ΔH_c) values were determined as the integral of their corresponding peaks, while the relative melting and crystallization enthalpy values of M6D within the nanocomposites were obtained by dividing ΔH_m by ΔH_c for the melting/crystallization enthalpy of the neat M6D capsules (equal to 158.4 J/g; see ref. [34]), taking into account the effective microcapsule concentration. Only one specimen was tested for each sample. Thermo-gravimetric analysis (TGA) was carried out with a TA Instruments TGA Q5000 thermobalance (TA Instruments, New Castle, DE, USA) under a nitrogen flow of 100 mL/min and in a temperature range from 30 °C to 700 °C at a heating rate of 10 °C/min. Only one specimen was tested for each composition. Dynamical mechanical analysis (DMA) was carried out using a TA Instruments DMA Q800 (TA Instruments, New Castle, DE, USA) analyzer in tensile configuration, testing rectangular 3D-printed specimens 30 mm long, 5 mm wide, and 1 mm thick. The testing temperature range was set between −60 °C and 100 °C, the heating rate was equal to 3 °C/min, the testing frequency was 1 Hz, and the strain amplitude was 0.05 mm/mm. Using this approach, the trends of the dynamic moduli (E' , E'') and the loss tangent ($\tan\delta$) as a function of temperature were highlighted. Moreover, the glass transition temperature of the TPU (T_g) was determined to be the inflection point of E' curves. Only one specimen was tested for each composition.

The mechanical behavior of the 3D-printed materials was investigated through quasi-static tensile tests conducted at room temperature, carried out according to ASTM D638 standard [40] using an Instron 5969 universal tensile testing machine (Instron, Norwood, MA, USA) equipped with a load cell of 50 kN. All samples were tested with a crosshead speed of 100 mm/min. A long-travel extensometer Instron 2603-080, with a gauge length of 25 mm, was used to monitor deformation during the tests. At least five specimens were tested for each composition in order to determine the chord modulus at a deformation of 10% and the stress and the strain at break. The specific fracture energy, representing the energy required for material failure divided by the cross-sectional area, was also determined. Creep tests were conducted using a TA Instruments DMA Q800 (TA Instruments, New Castle, DE, USA) in tensile configuration on rectangular 3D-printed specimens 30 mm long, 5 mm wide, and 1 mm thick (gauge length = 10 mm). The testing temperature was set to 30 °C, and a constant stress equal to 1 MPa was applied for 60 min. Only one specimen was tested for each composition.

The neat matrix was denoted as TPU, while the nanocomposites were named according to the matrix, the weight concentration of PCM (30 wt%, 40 wt%), and the MWCNT content (0.5 wt%, 1.0 wt%). For instance, TPU_30M6D_1MWCNT denotes the sample with 30 wt% microcapsules and 1 wt% carbon nanotubes. The M6D concentration was selected based on prior research findings in the field [26,33].

3. Results and Discussion

The cryofractured surfaces of 3D-printed samples of neat TPU and the relative composites were investigated using FESEM, and the most representative micrographs are provided in Figure 2a–d. Moreover, in Figure 3a–d, FESEM images at higher magnification are shown in order to highlight the microstructural details of the interphase between microcapsules and the TPU matrix. At low magnification, the 3D-printed TPU (Figure 2a) and TPU_1MWCNT (Figure 2b) specimens show a uniform and consistent arrangement of material layers deposited during the FFF process, with good adhesion between subsequent layers. Even in instances where the specimens were broken in liquid nitrogen, it is still possible to observe ductile fracture behavior due to the low glass transition temperature of TPU (about −50 °C). In the samples filled with microcapsules, a reduction in ductility is noticeable, with the appearance of a flat fracture profile, which can be attributed to the presence of M6D capsules acting as defects within the polymer matrix. This decreased ductility suggests compromised mechanical integrity and underscores the negative influence of the microcapsules on the failure properties of the resulting materials (Figure 2c,d). Nevertheless, it is possible to observe a triangularly shaped porosity corresponding to the edges of the filaments and good adhesion between the layers. No microcapsule agglomerates were detected, and the uniform M6D distribution allowed the morphological continuity of the

matrix to be retained even at elevated M6D concentrations. This feature could be important both for mechanical behavior and the thermal diffusivity of these samples.

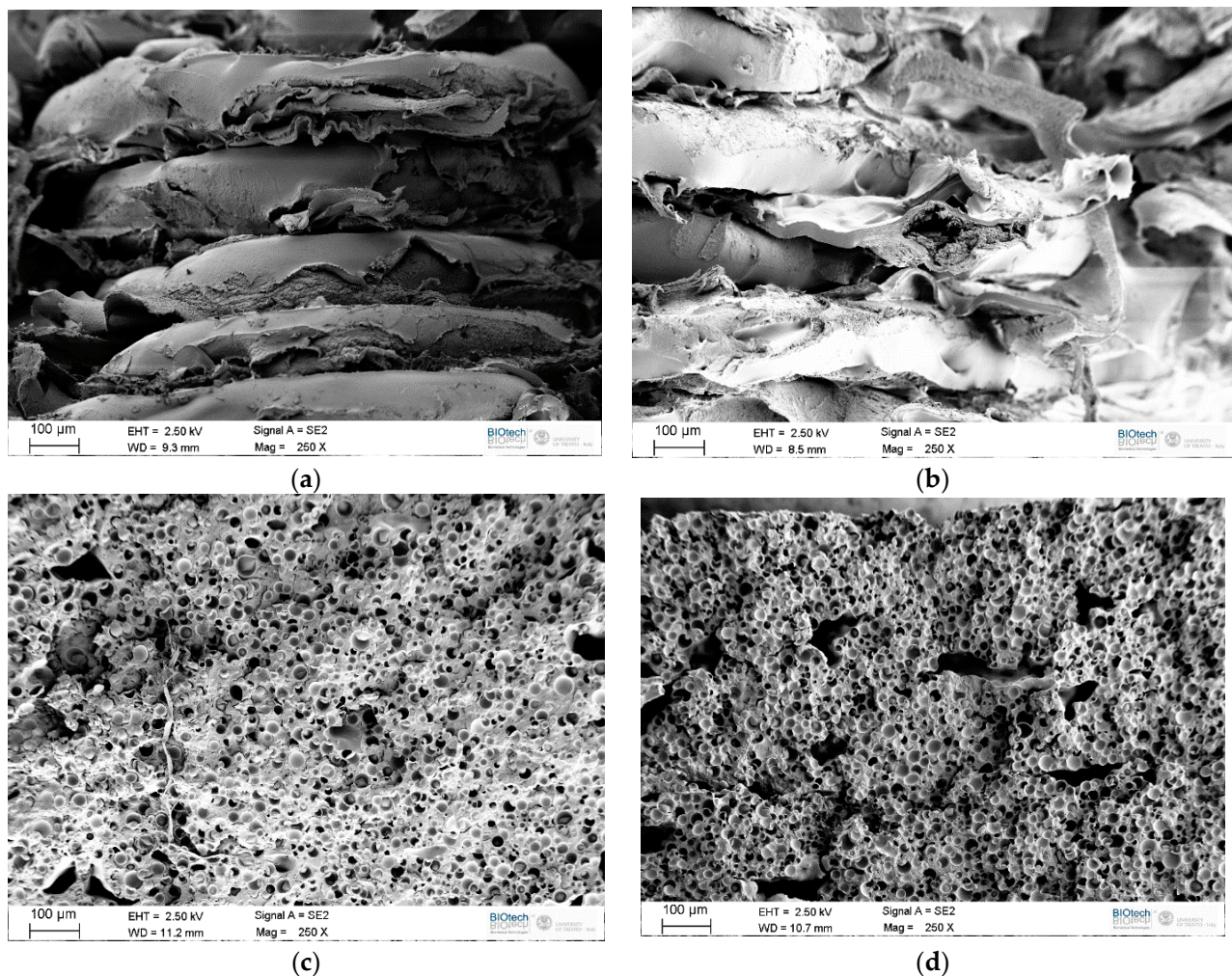


Figure 2. Low-magnification FESEM micrographs of 3D-printed (a) TPU, (b) TPU_1MWCNT, (c) TPU_30M6D_1MWCNT, and (d) TPU_40M6D_1MWCNT samples.

At higher magnification levels (see Figure 3a–d), some peculiar microstructural features can be detected. Even in the material containing microcapsules, the presence of a ductile fracture surface originating from the plastic deformation of the TPU matrix can be noticed. Upon a closer examination, an intriguing interplay becomes apparent: while the M6D shell demonstrates strong adherence to the TPU phase, it also exhibits a brittle behavior, as evidenced by the presence of sharp cracks traversing the surface of the capsule shell (see Figure 3c,d). Moreover, it is important to note that throughout the entire study, no agglomeration of MWCNTs was found within the TPU matrix. This observation emphasizes the successful integration of the MWCNTs into the composite material, contributing positively to the overall mechanical properties without compromising structural integrity. The reason for this brittleness can be traced back to the intrinsic brittle nature of the melamine shell the microcapsules are composed of. This observation underscores the complex interplay between the brittle behavior of the microcapsules' shells and their good interfacial interaction with the TPU matrix. These contrasting effects can strongly influence the failure behavior of the resulting materials.

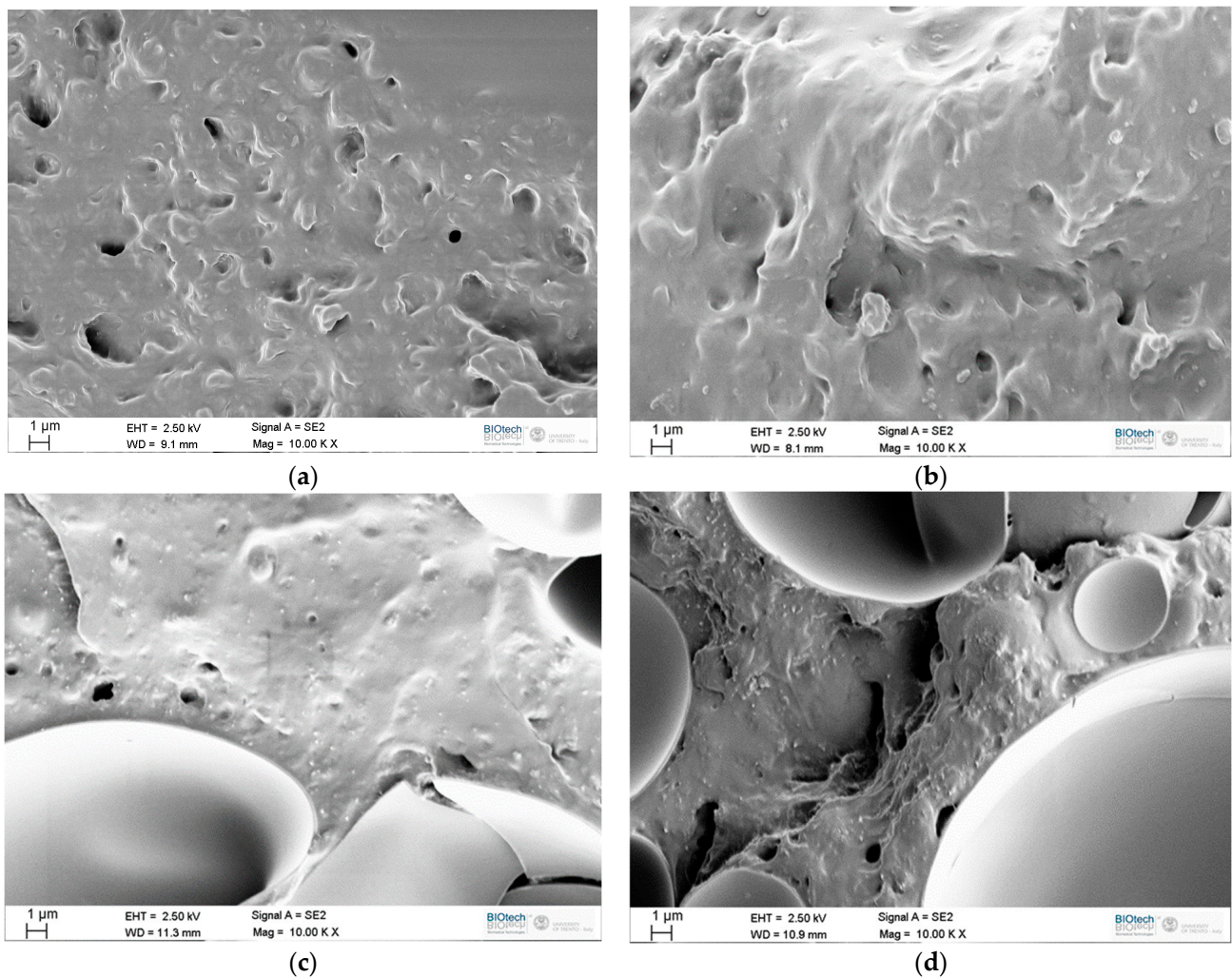


Figure 3. High-magnification FESEM micrographs of 3D-printed (a) TPU, (b) TPU_1MWCNT, (c) TPU_30M6D_1MWCNT, and (d) TPU_40M6D_1MWCNT samples.

In order to evaluate the thermal degradation resistance of the prepared nanocomposites, TGA was performed. In Figure 4a, thermogravimetric curves of neat TPU and the relative composites are shown, while in Figure 4b, the corresponding derivative thermogravimetric (DTG) curves are reported. At around 125 °C, there is an initial degradation step for the materials filled with microcapsules, and this mass loss (ranging from 2 wt% to 2.5 wt%) is proportional to the M6D content. This degradation step is related to the presence of residual paraffin leaking out from some microcapsules that broke during the manufacturing stage; this paraffin can easily evaporate at relatively low temperatures [34]. For all the samples, the major weight loss took place in the 280–485 °C range. From the DTG curves, it can be noticed that neat TPU degrades in 2 steps: the first peak, occurring at 335 °C, is related to the scission of urethane bonds, while the second peak, at 390 °C, corresponds to the dehydration reaction of the material produced by the scission of polyol segments [41]. The introduction of MWCNTs can slightly shift these two degradation steps towards higher temperatures. In particular, the first peak was shifted to 336 °C and 338 °C, while the second one was shifted to 391 °C and to 393 °C, when the samples had MWCNT content values of 0.5 wt% and 1 wt%, respectively. In the M6D-filled composites, the first degradation step of the TPU matrix coincides with the decomposition of the paraffin inside the microcapsules at 350 °C. The last degradation step detectable in the M6D-filled samples is located at 395 °C, and it is probably attributable to the presence of the crosslinked organic shells of the capsules, which have superior thermal resistance with respect to the TPU matrix. If the breakage of the microcapsules could be prevented, the thermal

degradation resistance of the composites would be comparable to that of TPU. It can therefore be concluded that the introduction of MWCNTs, resulting in a slight positive shift of the degradation steps, did not significantly compromise the overall thermal stability of the material. On the other hand, in the M6D-filled composites, the coincidence of the paraffin decomposition temperature with the TPU first degradation step, coupled with the decomposition of the crosslinked organic shells of the capsules at high temperatures, underscores the complex thermal degradation behavior of the prepared multifunctional composites. Further efforts will be made in the future to prevent microcapsule breakage and thus render the degradation resistance of the nanocomposites comparable to that of neat TPU.

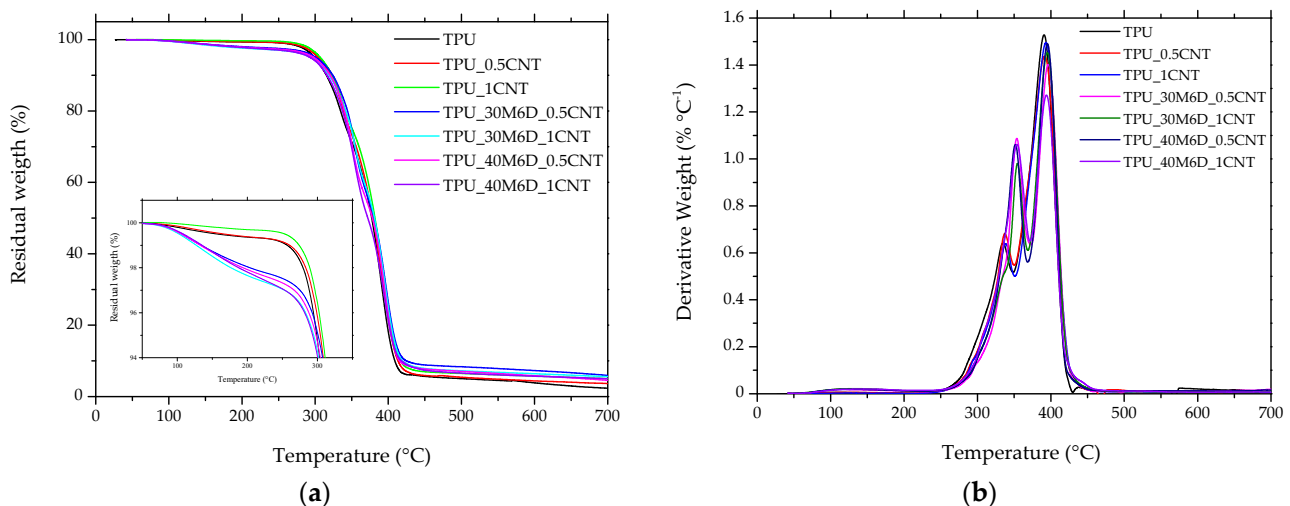


Figure 4. (a) TGA and (b) DTG curves from thermogravimetric analysis of the prepared 3D samples.

DSC is the main technique for evaluating the efficiency of materials that should be utilized for thermal energy storage applications, as it can give a precise measurement of the latent heat involved in phase-change transformations. In Figure 5a,b, DSC curves of the 3D-printed neat TPU and relative composites collected during the first heating step and the cooling scan, respectively, are reported, while the most important results are summarized in Table 1. This table also contains some results obtained in ref. [34] for neat capsules and TPU filled only with M6D capsules is reported for comparison. Neat TPU does not present any crystallization or melting peaks in the temperature range from -100 °C to 200 °C, and only an inflection point corresponding to the glass transition temperature (T_g) can be detected at -42 °C. This very-low T_g value determines the rubbery behavior of this material at room temperature. Regarding the composite samples, the melting peak is located at around 5 °C in the heating stage, while the crystallization peak is at about -8 °C in the cooling ramp. It can be noticed that both the melting and crystallization temperatures are only slightly affected by the introduction of M6D, and the limited T_m and T_c shifts can be attributed to the thermal inertia effect generated by the microcapsules [34,37]. The melting and crystallization enthalpy values are proportional to the M6D content and do not seem to be influenced by the presence of MWCNTs. However, the thermal energy storage efficiency of the prepared composites is relatively high, with the relative melting and crystallization enthalpies being higher than 80% for all the tested compositions. These efficiency values are consistent with the results previously found for TPU/M6D blends [34,37]. In order to increase the TES efficiency of these materials, milder processing conditions should be utilized in the future to retain the structural integrity of the microcapsules.

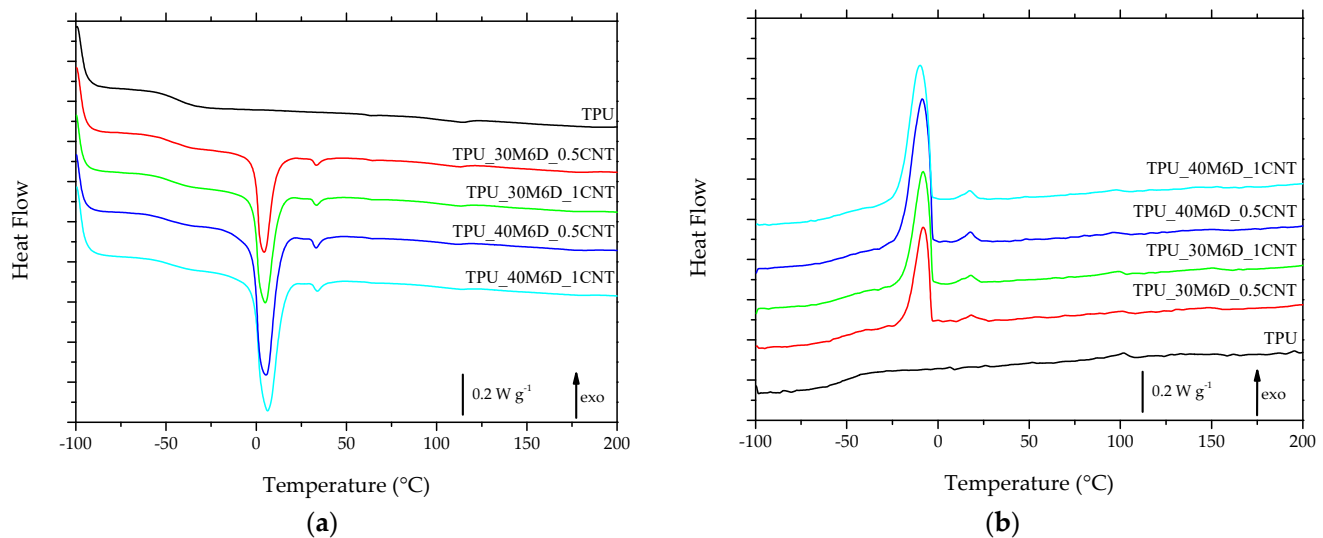


Figure 5. DSC thermograms of the prepared 3D-printed samples. (a) First-heating and (b) -cooling thermograms.

Table 1. Results of DSC tests on the prepared 3D printed samples.

	T_g (°C)	T_m (°C)	Melting Enthalpy (J/g)	Relative Melting Enthalpy (%)	T_c (°C)	Crystallization Enthalpy (J/g)	Relative Crystallization Enthalpy (%)
TPU	−48.9		−			−	
TPU_30 M6D *		6.6	45.6	28.8	−8.6	42.1	26.6
TPU_30M6D_0.5MWCNT		4.4	27.0	17.0	−1.1	29.1	18.4
TPU_30M6D_1MWCNT	−50.5	5.1	32.8	20.7	−2.1	37.4	23.6
TPU_40 M6D *		8.0	56.1	35.4	−10.1	52.6	33.2
TPU_40M6D_0.5MWCNT		5.4	48.7	30.7	−2.6	54.2	34.2
TPU_40M6D_1MWCNT	−53.9	6.4	47.6	30.0	−2.0	54.1	34.2
M6D *		5.0	158.5	100.0	−9.4	158.4	100.0

* Results from DSC tests reported in [34].

In sports applications or whenever a material is subjected to cyclic/vibrational load conditions, it is crucial to evaluate its viscoelastic behavior, which can be described through DMA tests in terms of storage modulus (E') and loss tangent ($\tan \delta$). In Figure 6a,b, the E' and $\tan \delta$ curves of the 3D-printed samples are shown, while in Table 2, the main results are summarized (the loss modulus (E'') curves are not reported for the sake of brevity). According to Figure 6a, at temperatures lower than -30 °C, there is a trend of a decrease in the storage modulus with a decrease in the microcapsule content, while this trend is the opposite at higher temperatures. Furthermore, from Figure 6b, it can be noticed that the intensity of the $\tan \delta$ peak decreases in tandem with the microcapsule content due to the lower TPU amount in the formulation. The storage modulus increased upon introducing MWCNTs in the temperature range considered; at room temperature, E' moves from 6.1 MPa for neat TPU up to 9.2 in the TPU_1MWCNT sample. Damping properties are influenced by the presence of microcapsules; in fact, the $\tan \delta$ peak at the TPU glass transition temperature decreased from the value of 0.80 for the neat TPU to 0.56 and 0.50 with M6D concentrations of 30 wt% and 40 wt%, respectively. The MWCNTs were able to slightly increase the glass transition temperatures compared to the neat TPU, while the microcapsules' introduction did not seem to substantially influence the T_g values, as already reported in the previous paper written by our group [34]. Furthermore, the incorporation of microcapsules inside the TPU matrix resulted in a shoulder in the E' and $\tan \delta$ curves located at about 10–15 °C, with a magnitude that increases in tandem with the M6D content. This signal is related to the melting of the paraffin wax within the microcapsules. It is thus clear that the viscoelastic response of these materials near ambient temperature could be strongly influenced by the melting of the paraffin inside the capsules.

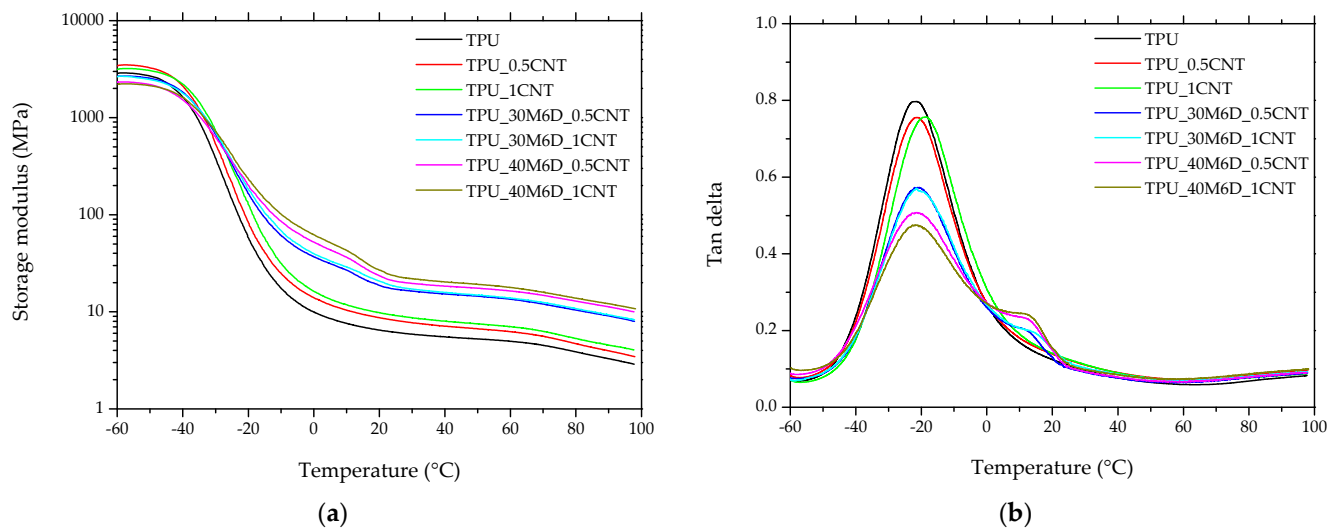


Figure 6. DMA thermograms of 3D-printed samples. Trends of (a) storage modulus (E') and (b) loss tangent ($\tan\delta$) as a function of the temperature.

Table 2. Results of DMA tests conducted on the prepared 3D-printed samples.

	T_g^* (°C)	E' at −60 °C (GPa)	E' at 25 °C (MPa)	$\tan\delta$ Peak Value
TPU	−39.3	2.856	6.1	0.80
TPU_0.5MWCNT	−37.9	3.134	8.1	0.75
TPU_1MWCNT	−36.5	3.422	9.2	0.75
TPU_30M6D_0.5MWCNT	−36.9	2.672	17.1	0.57
TPU_30M6D_1MWCNT	−36.4	2.647	18.3	0.56
TPU_40M6D_0.5MWCNT	−36.5	2.319	20.7	0.50
TPU_40M6D_1MWCNT	−33.3	2.206	23.4	0.47

* Evaluated as inflection point of E' curves.

Quasi-static tensile tests are important when evaluating the effect of microcapsules and MWCNTs in addition to the mechanical behavior of 3D-printed materials. The main mechanical properties of the prepared materials are summarized in Table 3. According to the ANOVA results, the addition of M6D significantly increased the stiffness of the 3D-printed samples (p -value = 10^{-9}), while the inclusion of MWCNTs had a positive but very limited effect that is statistically non-significant (p -value > 0.05), and this could be attributed to the low MWCNT content introduced (1 wt%). The enhancement in material stiffness at room temperature upon M6D introduction is attributable to the increased rigidity of the melamine shell containing the paraffin in the microcapsules [34]. On the other hand, the failure properties of the 3D-printed samples were negatively influenced by the presence of microcapsules, with an evident drop in both stress and strain at break upon the introduction of M6D. Consequently, the specific tensile energy at the breaking point is noticeably reduced. This reduction in ductility could be partly due to the non-optimal interfacial adhesion between the microcapsules and the TPU matrix. Also, the inclusion of MWCNTs in the TPU matrix engendered a reduction in the strain at break (p -value < 0.001), even if to a lower extent with respect to M6D addition. This embrittling effect could also be caused by a worsening of the printing quality and a consequent reduction in the effective cross-section, as observed in the SEM micrographs of the nanofilled samples (Figure 2).

In Figure 7, creep compliance curves of the 3D-printed samples at 30 °C are reported. Accordingly, compared to the results of the DMA and tensile tests, the dimensional stability clearly improved with the introduction of the MWCNTs, as the creep compliance value measured at 3600 s moved from 0.62 MPa^{-1} for the neat TPU up to 0.35 MPa^{-1} and 0.31 MPa^{-1} with a nanofiller content of 0.5 wt% and 1 wt%, respectively. Moreover, the simultaneous introduction of microcapsules and carbon nanotubes decreased the

creep compliance to 0.14 MPa⁻¹ in the TPU_40M6D_1MWCNT sample. It can also be interesting to fit creep data according to the existing models in the literature. In particular, the total creep compliance in terms of isothermal tensile creep in the linear viscoelastic region $D(t)$ is generally considered to consist of two components, with D_{el} representing the reversible and instantaneous elastic response and $D_{ve}(t)$ denoting the time-dependent viscoelastic response, if no plastic deformation is produced during the creep test, as reported in Equation (1) [42]:

$$D(t) = D_{el} + D_{ve}(t) \quad (1)$$

Table 3. Overview of Key Mechanical Properties for 3D-Printed TPU/MWCNT/PCM Composites: Modulus, Chord Stress at Break, Strain at Break, and Specific Energy at Break.

	Modulus Chord (MPa)	Stress at Break (MPa)	Strain at Break (mm/mm)	Specific Energy at Break (J/mm ²)
TPU	6.3 ± 0.4	9.1 ± 0.9	7.1 ± 0.5	0.90 ± 1.35
TPU_0.5MWCNT	7.8 ± 0.7	8.3 ± 1.1	6.1 ± 1.1	0.91 ± 1.77
TPU_1MWCNT	7.9 ± 0.5	7.6 ± 0.7	4.8 ± 0.3	0.62 ± 0.86
TPU_30M6D_0.5MWCNT	10.5 ± 1.0	5.2 ± 1.7	2.2 ± 0.5	0.29 ± 0.28
TPU_30M6D_1MWCNT	10.9 ± 0.4	5.3 ± 0.3	0.8 ± 0.1	0.08 ± 0.12
TPU_40M6D_0.5MWCNT	12.3 ± 0.8	4.9 ± 0.4	0.6 ± 0.1	0.05 ± 0.09
TPU_40M6D_1MWCNT	12.7 ± 0.1	3.8 ± 0.3	0.3 ± 0.1	0.01 ± 0.06

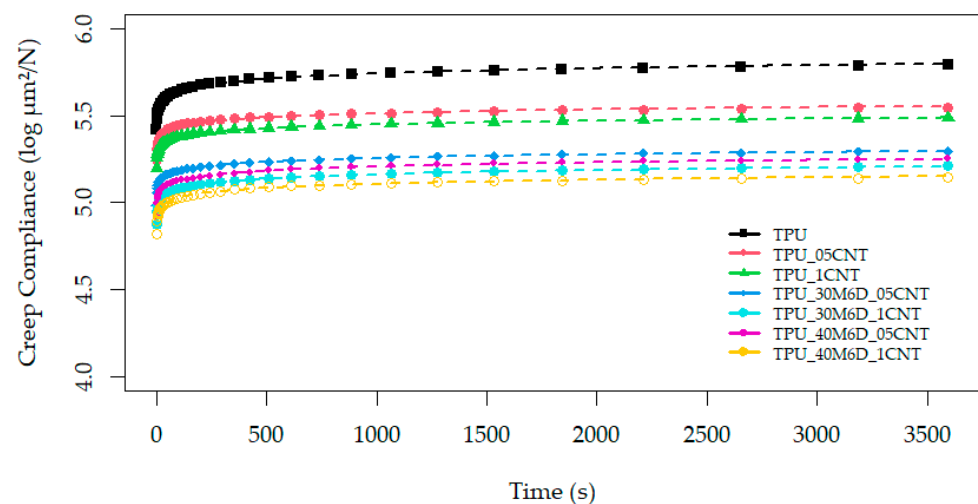


Figure 7. Creep compliance curves of 3D-printed samples, together with the fitting according to Findley's model (dotted lines (see Equation (2))).

In order to characterize the viscoelastic creep behavior, we used Findley's model, derived by extending the Kohlrausch–Williams–Watts (KWW) model, which is typically represented by a Weibull-like function in series form, with a focus on the primary term and disregarding the subsequent terms, as shown in Equation (2) [43]:

$$D(t) = D_{el} + kt^n \quad (2)$$

where k is a coefficient related to the magnitude of the underlying retardation process and n is an exponent tuning the time dependency of the creep process. The parameters derived from the fitting of the experimental creep data according to Findley's model are summarized in Table 4, together with the corresponding adjusted R-squared ($adj R^2$) values. As can be also noticed by examining the fitting of the creep compliance curves in Figure 7, the Findley model effectively captured the creep behavior of the prepared samples, displaying $adj R^2$ values higher than 0.995 for all the formulations. Moreover, the incorporation of MWCNTs and M6D led to a considerable decrease in both the D_{el} term

and the k coefficient, the latter being associated with the retardation of strain within the macromolecular structure [44]. The extent of this decrease is proportional to the nanofiller and microcapsule amounts. Also, the coefficient n , which represents the kinetics of the macromolecular flow during the creep process [45], experienced a reduction of about 30% with respect to neat TPU.

Table 4. Results of creep tests on the 3D-printed samples with fitting parameters based on Findley’s model (see Equation (2)).

	D_e (MPa ⁻¹)	k (MPa ⁻¹ s ⁻ⁿ)	n	Adj R ²
TPU	262,091	275,612 ± 1	0.1002 ± 0.0007	0.9980
TPU_0.5MWCNT	175,707	194,208 ± 1	0.0747 ± 0.0008	0.9960
TPU_1MWCNT	158,298	172,607 ± 1	0.0705 ± 0.0001	0.9998
TPU_30M6D_0.5MWCNT	96,351	110,359 ± 1	0.0709 ± 0.0003	0.9992
TPU_30M6D_1MWCNT	74,770	83,555 ± 1	0.0802 ± 0.0004	0.9988
TPU_40M6D_0.5MWCNT	83,523	93,255 ± 1	0.0790 ± 0.0005	0.9984
TPU_40M6D_1MWCNT	65,904	74,451 ± 1	0.0786 ± 0.0005	0.9985

4. Conclusions

Encapsulated paraffin and MWCNTs were successfully melt-compounded with TPU and processed via FFF to prepare novel multifunctional 3D-printed materials for thermal energy storage applications. FESEM analysis revealed a uniform dispersion of the microcapsules throughout the polymer matrix and strong adhesion between consecutive 3D-printed layers. However, as the concentrations of M6D and MWCNTs increased, the printing quality worsened, with the appearance of some layer misalignment and surface irregularities. TGA tests highlighted an initial degradation at 125 °C in the microcapsule-filled materials due to residual paraffin leaking out from damaged microcapsules, while the introduction of MWCNTs resulted in a slight positive shift in the degradation temperature. DSC tests revealed that the thermal energy storage efficiency of the 3D-printed materials was slightly lowered (about 20%) by the paraffin leakage caused by the compounding and FFF processes but remained at an interesting level (i.e., a melting enthalpy up to 48 J/g with an M6D content of 40 wt%). The stiffening effect provided by the MWCNTs and the microcapsules seen in the DMA was confirmed through quasi-static tensile tests. The limited TPU/M6D interfacial adhesion, coupled with the degradation of the printing quality observed in the MWCNT- and microcapsule-filled materials, led to an evident embrittlement and a consequent decrease in the failure properties. The addition of MWCNTs and PCM exerted a notable influence on creep behavior, with an evident reduction in both the elastic and the viscoelastic components of the creep compliance. Therefore, this study demonstrates the feasibility of utilizing additive manufacturing technology to fabricate 3D-printed materials based on TPU composites with thermal management capabilities. These multifunctional materials could find wide applications in innovative sectors such as sensors or in sport applications.

Author Contributions: Conceptualization, A.D. and A.P.; methodology, D.R.; software, D.R.; validation, D.R., A.D. and A.P.; formal analysis, D.R.; investigation, D.R.; resources, D.R.; data curation, D.R.; writing—original draft preparation, D.R.; writing—review and editing, A.D. and A.P.; visualization, D.R.; supervision, A.D. and A.P.; project administration, A.D. and A.P. All authors have read and agreed to the published version of the manuscript.

Funding: This research received no external funding.

Institutional Review Board Statement: Not applicable.

Informed Consent Statement: Not applicable.

Data Availability Statement: Dataset available on request from the authors.

Conflicts of Interest: The authors declare no conflicts of interest.

References

- Martin, D.J.; Osman, A.F.; Andriani, Y.; Edwards, G.A. 11—Thermoplastic polyurethane (TPU)-based polymer nanocomposites. In *Advances in Polymer Nanocomposites*; Gao, F., Ed.; Woodhead Publishing: Cambridge, UK, 2012; pp. 321–350.
- Drobny, J.G. 15—Applications of Thermoplastic Elastomers. In *Handbook of Thermoplastic Elastomers*; Drobny, J.G., Ed.; William Andrew Publishing: Norwich, NY, USA, 2007; pp. 281–315.
- Huang, C.; Qian, X.; Yang, R. Thermal conductivity of polymers and polymer nanocomposites. *Mater. Sci. Eng. R Rep.* **2018**, *132*, 1–22. [\[CrossRef\]](#)
- Hussain, A.R.J.; Alahyari, A.A.; Eastman, S.A.; Thibaud-Erkey, C.; Johnston, S.; Sobkowicz, M.J. Review of polymers for heat exchanger applications: Factors concerning thermal conductivity. *Appl. Therm. Eng.* **2017**, *113*, 1118–1127. [\[CrossRef\]](#)
- Kim, P.; Shi, L.; Majumdar, A.; McEuen, P.L. Thermal Transport Measurements of Individual Multiwalled Nanotubes. *Phys. Rev. Lett.* **2001**, *87*, 215502. [\[CrossRef\]](#)
- Spitalsky, Z.; Tasis, D.; Papagelis, K.; Galiotis, C. Carbon nanotube–polymer composites: Chemistry, processing, mechanical and electrical properties. *Prog. Polym. Sci.* **2010**, *35*, 357–401. [\[CrossRef\]](#)
- Tijing, L.D.; Park, C.-H.; Choi, W.L.; Ruelo, M.T.G.; Amarjargal, A.; Pant, H.R.; Im, I.-T.; Kim, C.S. Characterization and mechanical performance comparison of multiwalled carbon nanotube/polyurethane composites fabricated by electrospinning and solution casting. *Compos. B Eng.* **2013**, *44*, 613–619. [\[CrossRef\]](#)
- Fernández-d’Arlas, B.; Khan, U.; Rueda, L.; Martin, L.; Ramos, J.A.; Coleman, J.N.; González, M.L.; Valea, A.; Mondragon, I.; Corcuera, M.A.; et al. Study of the mechanical, electrical and morphological properties of PU/MWCNT composites obtained by two different processing routes. *Compos. Sci. Technol.* **2012**, *72*, 235–242. [\[CrossRef\]](#)
- Raja, M.; Ryu, S.H.; Shanmugaraj, A.M. Thermal, mechanical and electroactive shape memory properties of polyurethane (PU)/poly (lactic acid) (PLA)/MWCNT nanocomposites. *Eur. Polym. J.* **2013**, *49*, 3492–3500. [\[CrossRef\]](#)
- Bharadwaj, S.; Gupta, T.K.; Chauhan, G.S.; Sehrawat, M.; Kumar, A.; Dhakate, S.R.; Singh, B.P. Long Length MWCNT/TPU Composite Materials for Stretchable and Wearable Strain Sensors. *Sens. Actuators A Phys.* **2023**, *357*, 114364. [\[CrossRef\]](#)
- Jun, Y.-S.; Hyun, B.G.; Hamidinejad, M.; Habibpour, S.; Yu, A.; Park, C.B. Maintaining electrical conductivity of microcellular MWCNT/TPU composites after deformation. *Compos. B Eng.* **2021**, *223*, 109113. [\[CrossRef\]](#)
- Wang, X.; Xue, R.; Li, M.; Guo, X.; Liu, B.; Xu, W.; Wang, Z.; Liu, Y.; Wang, G. Strain and stress sensing properties of the MWCNT/TPU nanofiber film. *Surf. Interfaces* **2022**, *32*, 102132. [\[CrossRef\]](#)
- Kumar, S.; Gupta, T.K.; Varadarajan, K.M. Strong, stretchable and ultrasensitive MWCNT/TPU nanocomposites for piezoresistive strain sensing. *Compos. B Eng.* **2019**, *177*, 107285. [\[CrossRef\]](#)
- Rigotti, D.; Pegoretti, A. 23—Additive manufacturing with biodegradable polymers. In *Biodegradable Polymers, Blends and Composites*; Mavinkere Rangappa, S., Parameswaranpillai, J., Siengchin, S., Ramesh, M., Eds.; Woodhead Publishing: Cambridge, UK, 2022; pp. 611–679.
- Rigotti, D.; Fambri, L.; Pegoretti, A. Polyvinyl alcohol reinforced with carbon nanotubes for fused deposition modeling. *J. Reinf. Plast. Compos.* **2018**, *37*, 716–727. [\[CrossRef\]](#)
- Dul, S.; Fambri, L.; Pegoretti, A. Filaments production and fused deposition modelling of ABS/carbon nanotubes composites. *Nanomaterials* **2018**, *8*, 49. [\[CrossRef\]](#) [\[PubMed\]](#)
- Dul, S.; Ecco, L.G.; Pegoretti, A.; Fambri, L. Graphene/carbon nanotube hybrid nanocomposites: Effect of compression molding and fused filament fabrication on properties. *Polymers* **2020**, *12*, 101. [\[CrossRef\]](#) [\[PubMed\]](#)
- Dul, S.; Pegoretti, A.; Fambri, L. Fused Filament Fabrication of Piezoresistive Carbon Nanotubes Nanocomposites for Strain Monitoring. *Front. Mater.* **2020**, *7*. [\[CrossRef\]](#)
- Dul, S.; Fambri, L.; Pegoretti, A. Development of new nanocomposites for 3D printing applications. In *Structure and Properties of Additive Manufactured Polymer Components*; Friedrich, K., Walter, R., Soutis, C., Advani, S.G., Fiedler, I.H.B., Eds.; Woodhead Publishing: Cambridge, UK, 2020; pp. 17–59.
- Dorigato, A.; Moretti, V.; Dul, S.; Unterberger, S.H.; Pegoretti, A. Electrically conductive nanocomposites for fused deposition modelling. *Synth. Met.* **2017**, *226*, 7–14. [\[CrossRef\]](#)
- Dul, S.; Gutierrez, B.J.A.; Pegoretti, A.; Alvarez-Quintana, J.; Fambri, L. 3D printing of ABS Nanocomposites. Comparison of processing and effects of multi-wall and single-wall carbon nanotubes on thermal, mechanical and electrical properties. *J. Mater. Sci. Technol.* **2022**, *121*, 52–66. [\[CrossRef\]](#)
- Hohimer, C.J.; Petrossian, G.; Ameli, A.; Mo, C.; Pötschke, P. 3D printed conductive thermoplastic polyurethane/carbon nanotube composites for capacitive and piezoresistive sensing in soft pneumatic actuators. *Addit. Manuf.* **2020**, *34*, 101281. [\[CrossRef\]](#)
- Hohimer, C.; Aliheidari, N.; Mo, C.; Ameli, A. Mechanical Behavior of 3D Printed Multiwalled Carbon Nanotube/Thermoplastic Polyurethane Nanocomposites. In Proceedings of the ASME 2017 Conference on Smart Materials, Adaptive Structures and Intelligent Systems, Snowbird, UT, USA, 18–20 September 2017.
- Christ, J.F.; Aliheidari, N.; Ameli, A.; Pötschke, P. 3D printed highly elastic strain sensors of multiwalled carbon nanotube/thermoplastic polyurethane nanocomposites. *Mater. Des.* **2017**, *131*, 394–401. [\[CrossRef\]](#)
- Kim, K.; Park, J.; Suh, J.-h.; Kim, M.; Jeong, Y.; Park, I. 3D printing of multiaxial force sensors using carbon nanotube (MWCNT)/thermoplastic polyurethane (TPU) filaments. *Sens. Actuators A Phys.* **2017**, *263*, 493–500. [\[CrossRef\]](#)
- Cao, H. Smart coatings for protective clothing. In *Active Coatings for Smart Textiles*; Woodhead Publishing: Cambridge, UK, 2016; pp. 375–389.

27. Iqbal, K.; Khan, A.; Sun, D.; Ashraf, M.; Rehman, A.; Safdar, F.; Basit, A.; Maqsood, H.S. Phase change materials, their synthesis and application in textiles—A review. *J. Text. Inst.* **2019**, *110*, 625–638. [\[CrossRef\]](#)
28. Mondal, S. Phase change materials for smart textiles—An overview. *Appl. Therm. Eng.* **2008**, *28*, 1536–1550. [\[CrossRef\]](#)
29. Shim, H.; McCullough, E.A.; Jones, B.W. Using Phase Change Materials in Clothing. *Text. Res. J.* **2001**, *71*, 495–502. [\[CrossRef\]](#)
30. Gao, C. *Phase-Change Materials (PCMs) for Warming or Cooling in Protective Clothing*; Woodhead Publishing: Cambridge, UK, 2014; pp. 227–249.
31. Yazdi, M.; Sheikhzadeh, M.; Borhani, S. Modeling the heat transfer in a PCM cooling vest. *J. Text. Inst.* **2015**, *106*, 1003–1012. [\[CrossRef\]](#)
32. Abuzaaid, A.; Reichard, G. An Assessment of Utilizing Phase Change Materials (PCM) Towards Energy Performance in Building Enclosures. In Proceedings of the 3rd Residential Building Design & Construction Conference, State College, PA, USA, 2–3 March 2016.
33. Pielichowska, K.; Pielichowski, K. Phase change materials for thermal energy storage. *Prog. Mater. Sci.* **2014**, *65*, 67–123. [\[CrossRef\]](#)
34. Dorigato, A.; Rigotti, D.; Pegoretti, A. Thermoplastic Polyurethane Blends with Thermal Energy Storage/Release Capability. *Front. Mater.* **2018**, *5*. [\[CrossRef\]](#)
35. Rigotti, D.; Dorigato, A.; Pegoretti, A. Low-cycle fatigue behavior of flexible 3D printed thermoplastic polyurethane blends for thermal energy storage/release applications. *J. Appl. Polym. Sci.* **2021**, *138*, 49704. [\[CrossRef\]](#)
36. Khadiran, T.; Hussein, M.Z.; Zainal, Z.; Rusli, R. Encapsulation techniques for organic phase change materials as thermal energy storage medium: A review. *Sol. Energy Mater. Sol. Cells* **2015**, *143*, 78–98. [\[CrossRef\]](#)
37. Rigotti, D.; Dorigato, A.; Pegoretti, A. 3D printable thermoplastic polyurethane blends with thermal energy storage/release capabilities. *Mater. Today Commun.* **2018**, *15*, 228–235. [\[CrossRef\]](#)
38. ISO 527-1:2019; Plastics—Determination of Tensile Properties—Part 1: General Principles. International Organization for Standardization: Geneva, Switzerland, 2019.
39. Venkataraman, N.; Rangarajan, S.; Matthewson, M.J.; Harper, B.; Safari, A.; Danforth, S.C.; Wu, G.; Langrana, N.; Guceri, S.; Yardimci, A. Feedstock material property—Process relationships in fused deposition of ceramics (FDC). *Rapid Prototyp. J.* **2000**, *6*, 244–253. [\[CrossRef\]](#)
40. ASTM D638-14; Standard Test Method for Tensile Properties of Plastics. ASTM International: West Conshohocken, PA, USA, 2014.
41. Herrera, M.; Matuschek, G.; Kettrup, A. Thermal degradation of thermoplastic polyurethane elastomers (TPU) based on MDI. *Polym. Degrad. Stab.* **2002**, *78*, 323–331. [\[CrossRef\]](#)
42. Kolařík, J.; Pegoretti, A. Proposal of the Boltzmann-like superposition principle for nonlinear tensile creep of thermoplastics. *Polym. Test.* **2008**, *27*, 596–606. [\[CrossRef\]](#)
43. Dorigato, A.; Pegoretti, A. Tensile creep behaviour of polymethylpentene–silica nanocomposites. *Polym. Int.* **2010**, *59*, 719–724. [\[CrossRef\]](#)
44. Mahmood, H.; Vanzetti, L.; Bersani, M.; Pegoretti, A. Mechanical properties and strain monitoring of glass-epoxy composites with graphene-coated fibers. *Compos. A Appl. Sci. Manuf.* **2018**, *107*, 112–123. [\[CrossRef\]](#)
45. Dul, S.; Fambri, L.; Pegoretti, A. Fused deposition modelling with ABS–graphene nanocomposites. *Compos. A Appl. Sci. Manuf.* **2016**, *85*, 181–191. [\[CrossRef\]](#)

Disclaimer/Publisher’s Note: The statements, opinions and data contained in all publications are solely those of the individual author(s) and contributor(s) and not of MDPI and/or the editor(s). MDPI and/or the editor(s) disclaim responsibility for any injury to people or property resulting from any ideas, methods, instructions or products referred to in the content.